N7523921

NASA TM X-72692

NASA TECHNICAL
MEMORANDUM

NASA TM X-72692

RADIOMETRIC PERFORMANCE OF THE VIKING MARS

LANDER CAMERS

by Friedrich O. Huck, Ernest E. Burcher,
Edward J. Taylor, and Stephen D. Wall

NATIONAL AERONAUTICS AND SPACE ADMINISTRATION
LANGLEY RESEARCH CENTER, HAMPTON, VIRGINIA 23665

1 / 1

1. Report No. NASA TM X-72692	2. Government Accession No.	3. Recipient's Catalog No.
4. Title and Subtitle RADIOMETRIC PERFORMANCE OF THE VIKING MARS LANDER CAMERAS		5. Report Date APRIL 1975
		6. Performing Organization Code
7. Author(s) Friedrich O. Huck, Ernest E. Burcher, Edward J. Taylor, and Stephen D. Wall		8. Performing Organization Report No.
		10. Work Unit No.
9. Performing Organization Name and Address NASA Langley Research Center Hampton, VA 23665		11. Contract or Grant No.
12. Sponsoring Agency Name and Address National Aeronautics and Space Administration Washington, DC 20546		13. Type of Report and Period Covered Technical Memorandum
		14. Sponsoring Agency Code

15. Supplementary Notes

16. Abstract

The Viking lander cameras feature an array of 12 silicon photodiodes for electronic focus selection and multispectral imaging. Comparisons of absolute radiometric calibrations of the four cameras selected for the mission to Mars with performance predictions based on their design data reveal minor discrepancies. These discrepancies are caused primarily by the method used to calibrate the photosensor array and apparently also from light reflections internal to the array. The sensitivity and dynamic range of all camera channels are found to be sufficient for high-quality pictures providing that the commandable gains and offsets can be optimized for the scene radiance; otherwise, the quantization noise may be too high or the dynamic range too low for an adequate characterization of the scene.

ORIGINAL PAGE IS OF POOR QUALITY

17. Key Words (Suggested by Author(s)) (STAR category underlined) Radiometry Viking lander camera	18. Distribution Statement Unclassified - Unlimited

19. Security Classif. (of this report) Unclassified	20. Security Classif. (of this page) Unclassified	21. No. of Pages 50	22. Price*

RADIOMETRIC PERFORMANCE OF THE

VIKING MARS LANDER CAMERAS

By

Friedrich O. Huck, Ernest E. Burcher,

Edward J. Taylor*, and Stephen D. Wall

SUMMARY

The Viking lander cameras feature an array of 12 silicon photodiodes for electronic focus selection and multispectral imaging. Performance predictions based on detailed design and component calibration data of the four cameras selected for the mission to Mars are compared to absolute radiometric calibrations which are estimated to be accurate to ± 8 percent. The camera signal levels obtained during calibrations are found to be higher than the predicted signal levels by an average of 20 percent for the five broadband channels used for high-resolution imaging and rapid surveys, and 28 percent for the six narrowband channels used for multispectral imaging. (A channel for scanning the sun is not evaluated.) Investigations with a laboratory facsimile camera confirm that photosensor array signals should be about 18 percent higher than predicted because of different methods used to calibrate the photosensor arrays and the cameras. Additional variations which exist between the predictions and measurements may be caused by light reflections internal to the array.

Results of the calibrations are used to predict the cameras performance on Mars. Extensive tables are presented of the cameras sensitivity which

*General Electric Viking Support Office

varies with angular resolution, spectral responsivity, scan rate, and gain setting. The cameras sensitivity and dynamic range are sufficient for high-quality pictures providing that the commandable gains and offsets can be optimized for the scene radiance; otherwise, the quantization noise may be too high or the dynamic range too low for an adequate characterization of the scene.

INTRODUCTION

The Viking lander cameras feature an array of 12 silicon photodiodes, consisting of four broadband channels with selectable focus for high-resolution imaging, one broadband channel for low-resolution surveys, six narrowband channels for multispectral imaging (color and near-infrared), and one narrowband channel for scanning the sun. The instantaneous fields of view are 0.04° for the high-resolution channels and 0.12° for the other channels. The field of view in elevation ranges from 40° above to 60° below the horizon, and in azimuth ranges to 342.5°. High sensitivity is obtained over a wide dynamic range with only 6-bit encoding by use of 6 linear gains and 32 offsets. The cameras scanning rates are synchronized to the lander data transmission rates of 16,000 bits per second to two orbiters as relay stations and 250 bits per second directly to Earth.

The use of single photodiodes to scan the entire terrain provides the potential for good radiometric accuracy, and the use of six narrowband spectral channels provides a means for characterizing surface albedo. To fully realize these capabilities requires a careful radiometric evaluation and calibration of the cameras.

Six flight-qualified cameras have been fabricated: two cameras for each one of the two landers, and two spares. The assignment of these cameras to the two landers is as follows: cameras 1B and 2A are mounted on lander 1, and cameras 3A and Spare are mounted on lander 2. This apparently curious assignment of the cameras arose from their early designation by intended use (which then included also a third flight-qualified lander), and their later selection by overall performance.

A general description of the cameras design and performance characteristics is presented in reference 1. This paper presents a more detailed characterization of the radiometric response of the four flight cameras. This characterization essentially consists of comparing camera performance predictions with calibrations for all photosensor array channels (except the sun diode). The predictions are based on camera design data, such as lens transmittance, photosensor responsivity, and amplifier gain. The calibrations are obtained by imaging a reference test chart illuminated by a lamp that has been calibrated by the National Bureau of Standards (NBS). The ratios of measured over predicted signal magnitudes at the photosensor array output are used as calibration factors for predicting the cameras performance on Mars. Predictions are made with the camera performance prediction program described in reference 2.

SYMBOLS

c_n correction factor for radiometric calibration fixture

D diameter, m

f lens focal length

g phase angle, deg

G	gain of summing amplifier
G.n.	gain number
I	current, A
k	calibration factor
L	distance from camera lens in object space, m
ℓ	distance from camera lens in image space, m
$N(\lambda)$	spectral radiance, $W\text{-}m^{-2}\text{-}sr^{-1}\mu m^{-1}$
NER	noise-equivalent radius, $W\text{-}m^{-2}\text{-}sr^{-1}$
O.n.	offset number
R_f	preamplifier feedback resistance, Ω
$R(\lambda)$	photosensor responsivity, $A\text{-}W^{-1}$
$\mathcal{R}(\lambda)$	radiance-to-voltage conversion factor, $V\text{-}cm^2\text{-}W^{-1}$
r_a	photosensor aperture radius, m
$r_m(\lambda)$	mirror reflectance
$S(\lambda)$	irradiance, $W\text{-}m^{-2}\text{-}\mu m^{-1}$
V	voltage, V
W	noise-equivalent bandwidth, Hz
β	instantaneous field of view, deg or rad
ϵ	angle between emitted radiation and normal to surface, deg
ι	angle between incident radiation and normal to surface, deg
κ	number of quantization levels
λ	wavelength, μm
$\rho(\lambda)$	spectral reflectivity of surface (normal albedo)
$\tau(\lambda)$	spectral transmittance
$\tau(\lambda;\iota_o)$	spectral transmittance of atmosphere
ϕ	illumination scattering function

Subscripts:

a   photosensor aperture

c   photosensor array channel

co   commandable offset

cw   contamination cover

e   electronics

g   gain

i   integer

ℓ   lens

m   mirror

n   noise

o   fixed offset

pw   photosensor array window

q   quantization

w   window

CALIBRATION OF RADIOMETRIC RESPONSE

Performance Predictions

Signal.- Figure 1 presents a simplified cutaway view of the camera. The camera has two windows. The outer window, referred to as the contamination cover and not shown in figure 1, can be opened by a camera command. Light which passes through the inner window is reflected by a scanning mirror and focused by a lens onto a photodiode array. The photodiodes convert the light into a small electrical current which is amplified by preamplifiers and a summing amplifier as shown in figure 2. The resultant output voltage is given by (ref. 2)

$$V = k_c (\tfrac{\pi}{4})^2 \beta^2 D_\ell^2 R_f G \int_o^\infty N(\lambda)\tau_{cw}(\lambda)\tau_w(\lambda)\ r_m(\lambda)\tau_\ell(\lambda)\tau_{pw}(\lambda)\tau_f(\lambda)R'(\lambda)d\lambda \qquad (1)$$

where k_c is the calibration factor for each PSA channel (which is to be determined), β the instantaneous field of view, $D_\ell (=0.95$ cm) the lens diameter, R_f the preamplifier feedback resistance, G the channel gain, $N(\lambda)$ the object radiance, $\tau_{cw}(\lambda)$ and $\tau_w(\lambda)$ the contamination cover and window transmittance, $r_m(\lambda)$ the mirror reflectance, $\tau_\ell(\lambda)$ the lens transmittance, $\tau_{pw}(\lambda)$ the photosensor array window transmittance, $\tau_f(\lambda)$ the spectral filter (if present) transmittance, $R'(\lambda)$ the photodiode responsivity, and λ wavelength.

The instantaneous field of view is given by

$$\beta = 2 \tan^{-1}(\frac{r_a}{\ell_a}) \approx \frac{2r_a}{\ell_a} \qquad (2)$$

where r_a is the radius of the photodiode aperture and ℓ_a its distance from the lens. The in-focus object distance from the lens, L_a, is related to ℓ_a by the thin-lens formula

$$\frac{1}{f} = \frac{1}{L_a} + \frac{1}{\ell_a} \qquad (3)$$

where $f(=5.38$ cm) is the lens focal length. The in-focus object distances are 3.7 m for the low-resolution photodiodes, and 1.9, 2.7, 4.5, and 13.3 m for the high-resolution photodiodes.

The channel gain is the ratio of the summing amplifier feedback resistance (100 kΩ) to the input resistance R_i for each channel. These input resistances were selected to compensate for different photosensor aperture

sizes and filter transmittances, and for the spectral variation of the average Mars radiance.

The spectral radiance is given by

$$N(\lambda) = \frac{1}{\pi} S(\lambda)\tau(\lambda;\iota_o)\rho(\lambda)\phi(\epsilon,\iota,g;\lambda) \qquad (4)$$

where $S(\lambda)$ is the irradiance, $\tau(r;\iota_o)$ the atmospheric transmittance, $\rho(\lambda)$ and $\phi(\epsilon,\iota,g;\lambda)$ the scene albedo and illumination scattering function, respectively.

Independent filter transmittance, $\tau_f(\lambda)$, and photodiode responsivity, $R'(\lambda)$, measurements are not available. It is therefore convenient to let $R(\lambda) = \tau_{pw}(\lambda)\tau_f(\lambda)R'(\lambda)$ be the effective responsivity for each photodiode.

The output from the photosensor array is passed either directly (for the rapid-scan mode) or through a low-pass filter (for the slow-scan mode) to video processing electronics which provide commandable gains and offsets, automatic dark current subtraction, and analog-to-digital (A/D) conversion. Figure 3 shows a simplified block diagram of these circuits, and figure 4 the nominal 6 gains and 32 offsets. The transmitted digital number, DN, is related to the photosensor array output voltage by

$$DN = \frac{k_g}{2^{G.n.}} (V - k_{co} O.n. + k_o) \qquad (5)$$

where $G.n.$ is the gain number (ranging from 0 to 5), $O.n.$ the offset number (ranging from 0 to 31), k_g the gain constant (in DN/V), k_{co} the commandable offset constant, and k_o the fixed offset.

Noise.- The combined filtering of the analog video circuits results in a
noise-equivalent bandwidth of 2.8 kHz for the rapid-scan mode and 55 Hz for
the slow-scan mode. The quantization of the analog signal for digital
transmission generates a so-called quantization noise with a mean-square value
of

$$V_q^2 = \frac{\Delta V^2}{12\kappa^2} = \frac{1}{12\kappa^2} \left(\frac{63}{k_g} 2^{G.n.}\right)^2 \approx \frac{1}{12}\left(\frac{2^{G.n.}}{k_g}\right)^2 \tag{6}$$

where κ (=64) is the number of quantization levels and ΔV the dynamic range.
By combining electronic and quantization noise, the total root-mean-square
(rms) noise magnitude referred to the photosensor array output becomes

$$V_n = \sqrt{(I_e R_f G)^2 W + V_q^2} \tag{7}$$

where I_e is the electronic noise current per square-root hertz referred to
the photodiode output, and W the noise-equivalent bandwidth.

Sensitivity.- A common measure of sensitivity is the signal-to-rms-noise
ratio, V/V_n, where V is the photosensor array signal given by equation (1),
and V_n the total rms noise referred to the photosensor array output given by
equation (7). A related performance parameter is the noise-equivalent
radiance, NER, given by

$$NER = \frac{V_n}{V} \int_0^\infty N(\lambda) d\lambda \tag{8}$$

Input data.- Table I lists the window transmittance $\tau_{cw}(\lambda)$ and $\tau_w(\lambda)$ which are identical, the mirror reflectance $r_m(\lambda)$, and the lens transmittance $\tau_\ell(\lambda)$. Negligible variations were found to occur between samples so that these values can be used for all cameras.

The method of the photosensor array calibrations is described in reference 3. The results are given in terms of an overall photosensor array radiance-to-voltage conversion factor $\mathscr{R}(\lambda)$ (in V-cm^2/W) which is related to the photodiode responsivity $R'(\lambda)$ (in A/W) by

$$\mathscr{R}(\lambda) = \tau_{pw}(\lambda)\tau_f(\lambda)R'(\lambda)(\pi r_a^2)R_f G \tag{9a}$$

To account for the photosensor array characteristics, it is convenient to let

$$R(\lambda) = \tau_{pw}(\lambda)\tau_f(\lambda)R'(\lambda) = \frac{\mathscr{R}(\lambda)}{(\pi r_a^2)R_f G} \tag{9b}$$

The window transmittance $\tau_{pw}(\lambda)$ is 0.96 over the silicon photodiode responsivity range. Typical responsivities $R(\lambda)$ are plotted in figure 5; actual values deviate from these typical curves and are listed in Table II. Values of feedback resistances R_f, channel gains G, photodiode aperture radii r_a, and photodiode and preamplifier noise currents are listed in Table III.

Calibrations of gains and offsets are given in reference 4. Nominally, as shown in figure 6, the gain constant k_g should be 403.2 DN/V, the commandable offset intervals k_{co} should be 0.156 V, and the fixed offset k_o should be 0.216V. Actual values vary appreciably among cameras, and to a lesser extent in each camera as a function of gain, offset, and temperature. Only the gain and offset differences between cameras are accounted for in

predicting the cameras performance; average values of k_g, k_{co}, and k_o for each camera are listed in Table IV. Radiometric decalibrations of the camera data performed by the RADCAM program (ref. 5) also account for the variations of k_g, k_{co}, and k_o with gain, offset, and temperature.

Calibration Measurements

The absolute radiometric response of the cameras on Mars will be verified by the use of three identical reference test charts located on top of the lander. Each camera can view two of these charts at a distance of about 1 m. The charts (see fig. 6) provide 11 reflectance references (grey patches) varying in reflectance from 9.5 to 76 percent, three color patches to aid color reconstruction of images, and three tribars to check the camera frequency response. The illumination scattering function is approximately Lambertian (within $\pm$ 3 percent) for incident angles, ι, between 10° to 70° (i.e., the reflectance is proportional to $\cos \iota$, where $10^o \leq \iota \leq 70^o$).

The cameras are calibrated before flight against a reference test chart which, in turn, is illuminated by a lamp that has been calibrated by the National Bureau of Standards (NBS). A special calibration fixture is used to insure that the lamp-to-chart distance (0.5 m) and the illumination ($\iota = 20^o$) and viewing ($\epsilon = 0^o$) angles remain constant for all measurements. The fixture itself is also calibrated to account for peculiarities of lighting geometry and for internal reflections which occur despite careful baffling.

Four major error sources are as follows:

Lamp irradiance	$\pm$3 percent
Reference test chart reflectances	$\pm$6 percent·
Fixture	$\pm$3 percent
Camera gains and offsets.	$\pm$3 percent
Root-sum-square error	$\pm$8 percent

The lamp irradiance was calibrated by NBS to an accuracy of ± 3 percent in the spectral range of 0.4 to 1.1 μm (ref. 6).

The reference test chart reflectances were measured relative to magnesium carbonate ($MgCO_3$) for which the absolute reflectance in this spectral range is known with an accuracy of ± 3 percent (ref. 7). Errors introduced by not carefully accounting for some of the variations of this reflectance with wavelength and with lighting and viewing geometry, both in measuring the reference test chart reflectances and in using this reflectance data, diminishes the accuracy to ± 6 percent. To measure and use reference test chart reflectances more accurately would significantly increase calibration complexity. The reflectances ρ_n of the 11 grey patches are given in Table V, together with the correction factor c_n for each grey patch position in the calibration fixture. The reflectances represent the average value of measurements of three reference test charts; the measured reflectances varied less than ± 3 percent from these average values. These variations are within measurement errors and are neglected.

Flight camera calibrations were made at the Itek Corporation during May and June, 1974, and again at the Martin Marietta Corporation (MMC) during September to November, 1974. Two different calibration fixtures were used, each with its own lamp. The lamp irradiances are given in Table VI. Variations of the correction factors c_n between the two calibration fixtures were smaller than the uncertainty in their measurement. However, to reduce the effect of this error an average of all 11 grey scale calibration measurements is used to obtain the photosensor array calibration factors k_c.

The gain and offset constants k_g, k_{co}, and k_o vary independently with gains, offsets, and temperature (-41 to $+10^\circ$ C) by less than ± 2 percent

around their average value (listed in Table IV) for each camera; the total error is about ± 3 percent. One exception exists: the gain constant k_g for gain number 0 differs much more from this value; however, this gain was not used to obtain calibration data.

Results of the Itek and MMC calibration measurements are in close agreement, and only the MMC measurements presented in Tables VII are used. All measurements were obtained with the contamination cover open. The digital numbers, DN, are related to the photosensor array output voltages, V, by equation (5). Solving for V yields

$$V = c_n \frac{2^{G.n.}}{k_g} DN + k_{co}O.n. - k_o \tag{10}$$

Comparison of Performance Predictions

and Calibration Measurements

Performance predictions and calibration measurements are compared in Tables VIII. Tables VIII-A to D list the measured voltages (V_m), predicted voltages (V_p), and their ratios (V_m/V_p) for each photosensor array channel and each reference test chart grey patch. Blank spaces indicate that the grey patch radiance was outside the commanded camera dynamic range. The ratios V_m/V_p for each channel are averaged over the grey patches for which data is available to arrive at the photosensor array calibration factors k_c, which are summarized in Table VIII-E.

The comparison of measured and predicted photosensor array signal voltages, as given by the calibration factors k_c (see eq. (1)), reveals the following general results:

1. The calibration factors k_c are consistently larger than unity.

2. The average value of k_c for all photosensor array channels is 1.24, for all broadband channels is 1.20, and for all narrowband channels is 1.28.

3. The calibration factors k_c for the broadband channels range from 1.11 to 1.30 (i.e., ± 8 percent from their average value), and for the narrowband channels range from 1.02 to 1.52 (i.e., ± 20 percent from their average value.)

4. The average value of the calibration factor k_c for all channels of camera 1B is 1.22, for camera 2A is 1.23, for camera 3A is 1.32, and for camera Spare is 1.18.

Results described in the Appendix suggest that a calibration factor k_c of about 1.2 may be expected because of a basic difference in the method used for calibrating the photosensor arrays and the cameras. Systematic errors between cameras (e.g., $k_c \geq 1.35$ for all green channels) may be caused by light reflections internal to the array, while random errors may be expected because of resistance tolerances, especially of the preamplifier feedback resistors.

PERFORMANCE PREDICTIONS WITH

CALIBRATED RADIOMETRIC RESPONSE

The radiometric performance of the cameras is predicted for the Mars environment, using the photosensor array calibration factors k_c determined in the foregoing section. All predictions are made for the average Mars radiance data listed in Table IX.

Signal Level and Dynamic Range

Reference test chart.- Table X lists the photosensor array output voltages when the cameras view a reference test chart. The sun incidence angle, ι, is assumed to be 60°; the illumination scattering function of the grey patches is approximately Lambertian for incidence angles ranging between 10° to 70° (i.e., the reflectance is proportional to $\cos \iota$ where $10^\circ \leq \iota \leq 70^\circ$). The effect of light reflections off the lander structure onto the reference test chart, which might be appreciable at large incident angles, has not been investigated.

Voltages are given for the 40% reflectance grey patch. Together, the 11 grey patches would provide reference voltages ranging from about one-fourth to twice these values, covering most of the dynamic range of the camera which extends to 7.28 V.

Mars surface.- Table XI lists the photosensor array output voltages obtained for the average Mars radiance and an illumination scattering function equal to unity (i.e., $\phi(\varepsilon,\iota,g;\lambda) = 1$). The average value of the output voltages is 1.46 V, which is 12 percent higher than the design goal of 1.28 V. Variations around this average value range from 1.39 to 1.58 V (i.e., -5 to +8 percent) for the broadband channels, and from 1.25 to 1.78 (i.e., -15 to +22 percent) for the narrowband channels.

About 4 to 6 times the average Mars radiance can therefore be encompassed by the camera dynamic range. This range should generally be sufficient; yet, some constraints exist for the blue and green channels. The average Mars surface albedo is about 0.08 to 0.12 in the blue-green wavelength region (see Table IX), so that surface albedoes up to only about 0.3 to 0.6 can be imaged by the blue and green channels at high sun elevation or near-zero phase

angles (i.e., when $\phi(\epsilon,\iota,g;\lambda) \approx 1$). However, surfaces with higher albedoes could still be imaged at low sun elevations (i.e., when $\phi(\epsilon,\iota,g) < 0.5$).

Sensitivity

Noise-equivalent radiance.- Table XII presents the noise-equivalent radiances (NER) at the photosensor array output prior to quantization. These NER are not achievable since quantization is inevitable; however, these quantities are more sensitive indicators of the photosensor arrays performance than the NER after quantization. The results show that the sensitivities of the four cameras for corresponding channels are generally within ± 20 percent of their average value; exceptions are minor.

Table XIII presents a listing of NER (including quantization noise) for the five gain numbers and two scan rates. Camera 1B, with the channel BB2 as representative of the high-resolution channels, is used as example. The sensitivity of the other cameras falls within ± 26 percent of this example.

Signal-to-noise ratio.- Table XIV presents signal-to-rms-noise ratios (V/V_n) for all gain numbers and scan rates. The signal levels V are defined as the maximum signal level for the average Mars radiance, and are listed in Table XI. The average signal levels -- and hence the average-signal-to-rms noise ratios -- may be expected to range from about 1/2 of these values for high sun elevations to 1/4 or less for low sun elevations. Further variations will occur with surface albedo.

The signal-to-noise ratios for high gain numbers (4 and 5) and low sun elevations and/or surface albedos may easily be insufficient for adequate pictures. Yet high gain numbers are required for any preprogrammed camera commands to reasonably assure that most of the unknown radiance range will be encompassed. However, once the scene radiance has been approximately

characterized from initial pictures, camera gains and offsets can be readily optimized to provide sufficient signal-to-noise ratios for high-quality pictures, even if fairly low surface albedoes are encountered.

CONCLUSIONS

Predictions based on detailed design data of the four Viking lander cameras were compared to absolute radiometric calibrations, which, in turn, were estimated to be accurate to within ±8 percent. General results are:

1. The measured photosensor array signal is consistently higher than the predicted value. It is on the average 20 percent higher for the five broadband channels, and 28% for the six narrowband channels.

2. Signal variations around these average values are within ±8 percent for the broadband channels and within ±20 percent for the narrowband channels.

3. Investigations with a laboratory facsimile camera suggest that the measured signal should be about 18 percent higher than the predicted signal because of different methods used to calibrate the photosensor arrays and the cameras. However, the reason for this is not known. Additional variations which exist between the predictions and measurements may be primarily caused by light reflections internal to the array.

Using results of the calibrations to predict the cameras performance on Mars led to the following general results:

1. The photosensor array output signals for the average Mars radiance reach 1.46V on the average, which is 12 percent higher than the design goal of 1.28V.

2. Variations around this average signal level of 1.46V range from -5 to +8 percent for the broadband channels, and from -15 to +22 percent for the

narrowband channels.

3. The camera dynamic range of 7.28V encompasses about 4 to 6 times the average Mars radiance. While sufficient for most channels, the dynamic range constraints imaging with the blue and green channels to surface albedoes less than about 0.3 to 0.6 at high sun elevations. Higher surface albedoes must be imaged at low sun elevations.

4. .The sensitivity of corresponding photosensor array channels (e.g., of all blue channels) is within ±20 percent of the average value for the four cameras with only minor exceptions.

5. The cameras sensitivites are sufficient for high-quality pictures providing that camera gains and offsets can be optimized for the scene radiance that is encountered. Otherwise, either the quantization noise may be too high or the dynamic range too low for adequate characterizations of the Mars surface.

APPENDIX

PERFORMANCE PREDICTIONS AND CALIBRATION MEASUREMENTS
WITH A LABORATORY FACSIMILE CAMERA

It was found that the measured photosensor array output voltages of the four Viking lander cameras are consistently higher than their predicted values; in particular, that the average ratio of the measured over predicted voltage for all broadband channels is 1.20, and that the variations of this ratio are confined to the range extending from 1.11 to 1.30. The purpose of this appendix is to present results of an experiment that has been made with a laboratory facsimile camera to investigate the cause of this discrepancy.

A description of the laboratory facsimile camera has been presented in reference 2. However, it is pertinent to point out again that the photosensor of this camera consists of a single silicon diode which is rigidly mounted behind a small aperture inside a metal capsule which also contains the pre-amplifier. The photosensor capsule can be readily inserted and removed from the facsimile camera without disturbing any electrical connections or turning off any electrical power.

The first step of the investigation was to let the photosensor directly view a NBS-calibrated lamp. The photosensor output voltage was predicted by the relationship

$$V_o = \pi r_a^2 \, R_f \left(\frac{0.5}{L_o}\right)^2 \int_o^\infty S(\lambda)R(\lambda)d\lambda \qquad \text{(A-1)}$$

where r_a is the photosensor aperture radius, R_f the photodiode preamplifier feedback resistance, $R(\lambda)$ the photodiode responsivity, $S(\lambda)$ the lamp irradiance at a distance of 0.5 m, and L_o the photosensor-to-lamp distance. This test was repeated for several distances ($4m \leq L_o \leq 8m$). The resultant ratios of measurement to prediction were $1.03 \pm .02$.

The second step of the investigation was to insert the photosensor into the facsimile camera and image a magnesium oxide ($MgCO_3$) block illuminated by the same lamp. The photosensor output voltage was predicted using the relationship (similar to eq. (1))

$$V = 1.03 \left(\frac{\pi}{4}\right)^2 \left(\frac{2r_a}{\ell_o}\right)^2 D^2 R_f \int_o^\infty N(\lambda)r_m(\lambda)\tau_\ell(\lambda)R(\lambda)d\lambda \qquad \text{(A-2)}$$

where ℓ_a is the photosensor aperture distance from the lens, D the lens aperture diameter, $r_m(\lambda)$ the scanning mirror reflectance, and $\tau_\ell(\lambda)$ the lens transmittance. (No windows were used.) The spectral radiance of the $MgCO_3$ block is given by

$$N(\lambda) = \frac{1}{\pi} \left(\frac{0.5}{L_o}\right)^2 S(\lambda) \, \rho_{MgCO_3} \cos \iota \qquad \text{(A-3)}$$

where the silicon-responsivity-weighted reflectance of $MgCO_3$ is $\rho_{MgCO_3} = 0.968(\pm 0.025)$ (ref. 7). The camera viewing angle was normal to the flat surface of the $MgCO_3$ block. This test was repeated for several distances $(0.7 \le L_o \le 1.5 \text{ m})$, several illumination angles $(20° \le \iota \le 40°)$, and several surface textures of $MgCO_3$ (by preparing it with different-sized sandpapers). The resultant ratios of measurement over predictions were $1.18 \pm .05$. The reason for this is not known.

This result is consistent with the corresponding average ratio of 1.20 for all broadband channels of the Viking lander cameras. The Viking photosensor arrays were calibrated against a reference silicon photodiode which, in turn, was calibrated by a method which is essentially similar to the first step of this investigation. The Viking reference photodiode was calibrated at two laboratories: the Optics Laboratory of the Flight Instrumentation Division, LaRC, and the Air Force Cambridge Research Laboratory, Massachusetts. The two absolute radiometric measurements fell within ± 4 percent of their average value (ref. 8).

REFERENCES

1. Huck, F. O.; McCall, H. F.; Patterson, W. F.; Taylor, G. R.: The Viking Mars Lander Camera. To be published in Space Science Instrumentation.

2. Huck, F. O.; Taylor, E. J.; Jobson, D. J.; Rowland, C. W.: Performance and Evaluation of the Viking Lander Camera Performance Prediction Program. NASA TMX-72646, January 1975.

3. Acceptance Data Package for Photosensor Array. Martin-Marietta Documents for PSA Serial No. M15, M17, M19, M20. Science Team Data.

4. Wolf, M. R.: JPL/IPL Calibration Data Transmittal, Viking Lander Camera.

5. Wolf, M. R.: Software Requirements Document for the RADCAM Program. Viking Doc. No. 620-65, Rev. A, March, 1975

6. Stair, R., et al: A New Standard of Spectral Irradiance. Applied Optics, Vol. 2, Nov. 1963.

7. Measurements of Thermal Radiation Properties of Solids. NASA SP-31, 1963.

8. Personal communications with W. R. Patterson, Brown University.

TABLE I

OPTICAL CAMERA THROUGHPUT

λ, μm	τ_{cw}, τ_w	τ_m	τ_ℓ
.4	.926	.692	.931
.425	.930	.774	.945
.45	.932	.783	.959
.475	.934	.820	.964
.5	.940	.857	.963
.525	.940	.846	.966
.55	.945	.844	.954
.575	.945	.837	.953
.6	.949	.817	.955
.625	.948	.819	.950
.65	.950	.800	.943
.675	.949	.795	.942
.7	.949	.790	.947
.725	.948	.767	.934
.75	.948	.744	.945
.775	.947	.749	.926
.8	.948	.731	.920
.825	.947	.785	.916
.85	.947	.782	.914
.875	.944	.794	.904
.9	.943	.815	.895
.925	.945	.835	.892
.95	.945	.849	.890
.975	.947	.863	.882
1.0	.941	.870	.869
1.025	.945	.876	.873
1.05	.942	.880	.862
1.075	.942	.880	.861
1.1	.941	.881	.864

TABLE II-A

RESPONSIVITIES OF PHOTOSENSOR ARRAY M17 IN FLIGHT CAMERA 1B

RESPONSIVITY, A/W

λ, μm	BB1	BB2	BB3	BB4	SURVEY	BLUE	GREEN	RED	IR1	IR2	IR3
.350	.047	.052	.052	.055	.055	.005	.003	.000	.002	.002	.021
.375	.061	.051	.051	.054	.062	.011	.004	.002	.002	.004	.009
.400	.095	.095	.093	.104	.097	.044	.001	.005	.002	.002	.005
.425	.127	.125	.129	.122	.126	.082	.001	.004	.001	.001	.001
.450	.150	.149	.159	.153	.151	.120	.002	.002	.001	.001	.005
.475	.174	.172	.187	.138	.175	.142	.003	.001	.001	.002	.009
.500	.197	.196	.212	.215	.198	.120	.044	.001	.000	.008	.014
.525	.204	.201	.221	.226	.210	.004	.108	.001	.000	.017	.008
.550	.214	.215	.235	.240	.224	.001	.186	.001	.001	.007	.005
.575	.232	.236	.259	.236	.248	.001	.002	.003	.001	.001	.005
.600	.247	.253	.279	.286	.267	.001	.017	.053	.001	.001	.006
.625	.264	.270	.291	.305	.285	.002	.003	.252	.001	.001	.008
.650	.276	.232	.310	.317	.296	.014	.001	.251	.001	.001	.010
.675	.282	.220	.221	.327	.306	.037	.001	.235	.000	.001	.015
.700	.291	.228	.330	.335	.316	.005	.001	.222	.001	.002	.022
.725	.297	.307	.333	.345	.326	.001	.001	.187	.001	.005	.029
.750	.307	.315	.343	.352	.332	.001	.000	.040	.006	.007	.042
.775	.315	.323	.352	.356	.343	.000	.002	.024	.030	.002	.007
.800	.320	.328	.359	.267	.351	.002	.002	.010	.128	.002	.002
.825	.321	.330	.364	.375	.358	.000	.000	.007	.290	.002	.002
.850	.319	.327	.358	.370	.356	.000	.000	.003	.225	.005	.003
.875	.306	.314	.343	.353	.344	.000	.000	.007	.272	.025	.008
.900	.286	.293	.319	.329	.328	.001	.000	.001	.101	.220	.028
.925	.265	.272	.297	.305	.309	.000	.001	.000	.026	.270	.117
.950	.240	.244	.267	.275	.285	.001	.001	.000	.011	.138	.212
.975	.209	.213	.235	.239	.253	.003	.001	.000	.006	.027	.169
1.000	.159	.162	.179	.181	.195	.002	.003	.000	.004	.010	.121
1.025	.112	.114	.128	.127	.140	.002	.002	.001	.003	.005	.072
1.050	.067	.067	.078	.075	.083	.004	.002	.001	.003	.004	.038
1.075	.035	.034	.040	.038	.043	.018	.006	.000	.003	.004	.020
1.100	.018	.018	.021	.019	.021	.014	.016	.000	.004		

TABLE II-B

RESPONSIVITIES OF PHOTOSENSOR ARRAY M20 IN FLIGHT CAMERA 2A

RESPONSIVITY, A/W

λ, μm	BB1	BB2	BB3	BB4	Survey Blue	Blue	Green	Red	IR1	IR2	IR3
.350	.045	.049	.043	.048	.061	.003	.003	.004	.006	.008	.020
.375	.054	.053	.047	.057	.057	.010	.003	.002	.003	.004	.010
.400	.095	.088	.085	.094	.095	.041	.001	.005	.001	.002	.005
.425	.117	.110	.108	.124	.124	.083	.001	.005	.001	.001	.003
.450	.141	.134	.131	.145	.145	.118	.001	.002	.001	.001	.005
.475	.164	.158	.157	.172	.171	.141	.003	.001	.001	.002	.009
.500	.188	.182	.181	.198	.196	.150	.047	.001	.001	.009	.013
.525	.203	.195	.195	.213	.212	.005	.117	.001	.001	.019	.008
.550	.219	.209	.211	.230	.231	.001	.173	.001	.001	.007	.005
.575	.233	.223	.224	.243	.245	.001	.070	.003	.001	.001	.005
.600	.246	.235	.234	.254	.256	.001	.014	.046	.001	.001	.005
.625	.261	.250	.250	.271	.275	.002	.002	.234	.002	.001	.007
.650	.272	.259	.260	.282	.286	.009	.001	.241	.002	.001	.010
.675	.278	.265	.267	.289	.293	.032	.001	.255	.001	.001	.014
.700	.285	.273	.276	.298	.304	.006	.001	.285	.001	.001	.021
.725	.295	.279	.284	.307	.313	.001	.001	.194	.001	.002	.027
.750	.309	.292	.293	.316	.325	.001	.000	.046	.001	.005	.040
.775	.316	.300	.300	.324	.337	.000	.001	.027	.007	.008	.008
.800	.324	.306	.306	.329	.347	.002	.002	.011	.029	.003	.003
.825	.320	.306	.303	.329	.351	.000	.000	.008	.114	.002	.002
.850	.315	.301	.426	.324	.352	.000	.000	.003	.277	.003	.002
.875	.302	.288	.287	.312	.344	.000	.000	.008	.219	.006	.004
.900	.281	.268	.266	.289	.330	.000	.000	.001	.258	.026	.008
.925	.260	.249	.245	.258	.314	.001	.001	.000	.124	.198	.029
.950	.235	.223	.221	.240	.292	.000	.001	.000	.033	.262	.115
.975	.205	.195	.192	.208	.263	.001	.001	.001	.013	.158	.221
1.000	.156	.149	.209	.158	.206	.002	.002	.001	.007	.034	.182
1.025	.110	.105	.103	.111	.147	.002	.002	.000	.005	.012	.131
1.050	.065	.064	.061	.065	.088	.005	.002	.001	.004	.006	.079
1.075	.033	.034	.032	.034	.045	.019	.006	.000	.003	.004	.041
1.100	.017	.017	.016	.018	.023	.015	.017	.000	.004	.004	.022

TABLE II-C

RESPONSIVITIES OF PHOTOSENSOR ARRAY M15 IN FLIGHT CAMERA 3A

RESPONSIVITY, A/W

λ, μm	BB1	BB2	BB3	BB4	SURVEY BLUE	GREEN	RED	IR1	IR2	IR3
.900	.235	.253	.283	.253	.315	.001	.000	.046	.264	.040
.925	.221	.250	.252	.234	.295	.000	.000	.014	.253	.161
.950	.201	.226	.238	.213	.265	.000	.000	.007	.064	.225
.975	.177	.197	.207	.185	.206	.002	.000	.004	.018	.177
1.000	.136	.149	.159	.142	.149	.002	.001	.003	.009	.128
1.025	.097	.105	.114	.101	.088	.002	.001	.003	.006	.077
1.050	.056	.061	.068	.060	.046	.006	.000	.003	.005	.041
1.075	.029	.032	.035	.031	.023	.019	.000	.005	.037	.021
1.100	.015	.016	.019	.016	.013	.019	.000	.005	.037	.021

TABLE II-D

RESPONSIVITIES OF PHOTOSENSOR ARRAY M19 IN FLIGHT CAMERA SPARE

RESPONSIVITY, A/W

λ, μm	BB1	BB2	BB3	BB4	SURVEY	BLUE	GREEN	RED	IR1	IR2	IR3
.350	.066	.066	.064	.060	.067	.004	.003	.004	.006	.008	.021
.375	.079	.079	.075	.076	.072	.011	.004	.002	.003	.234	.212
.400	.122	.117	.116	.116	.106	.046	.001	.006	.002	.002	.005
.425	.150	.152	.151	.151	.140	.089	.001	.005	.001	.001	.004
.450	.178	.178	.173	.177	.167	.132	.001	.002	.001	.001	.005
.475	.207	.208	.202	.205	.195	.154	.003	.001	.001	.002	.012
.500	.235	.235	.231	.233	.223	.155	.045	.001	.001	.009	.014
.525	.244	.245	.237	.243	.236	.005	.097	.001	.001	.218	.227
.550	.260	.259	.252	.261	.254	.001	.168	.002	.001	.005	.005
.575	.284	.286	.276	.283	.279	.001	.065	.003	.001	.001	.004
.600	.299	.302	.291	.300	.296	.001	.013	.049	.001	.001	.005
.625	.316	.321	.313	.323	.319	.002	.003	.239	.002	.001	.007
.650	.331	.335	.324	.336	.332	.012	.001	.243	.002	.001	.010
.675	.339	.345	.334	.345	.342	.034	.001	.258	.001	.001	.014
.700	.351	.355	.343	.355	.354	.005	.001	.288	.001	.001	.021
.725	.359	.364	.351	.363	.361	.001	.001	.186	.001	.002	.022
.750	.376	.380	.366	.378	.376	.001	.000	.046	.002	.005	.047
.775	.387	.391	.377	.388	.389	.000	.001	.028	.007	.007	.039
.800	.393	.398	.384	.394	.401	.002	.002	.012	.028	.003	.003
.825	.388	.391	.385	.391	.403	.000	.000	.009	.122	.002	.002
.850	.385	.385	.379	.386	.400	.000	.000	.003	.246	.003	.002
.875	.370	.372	.365	.373	.391	.000	.000	.009	.197	.007	.003
.900	.344	.347	.341	.349	.373	.001	.000	.002	.227	.033	.007
.925	.317	.321	.317	.322	.356	.001	.001	.001	.078	.222	.022
.950	.285	.289	.287	.290	.330	.001	.000	.001	.022	.251	.094
.975	.249	.251	.252	.252	.298	.004	.001	.001	.010	.129	.231
1.000	.190	.191	.193	.191	.232	.003	.003	.001	.006	.029	.061
1.025	.134	.135	.139	.133	.167	.003	.002	.001	.005	.011	.137
1.050	.077	.078	.083	.058	.098	.006	.003	.001	.003	.006	.083
1.075	.040	.040	.044	.039	.050	.021	.026	.001	.003	.005	.043
1.100	.021	.021	.023	.020	.026	.018	.016	.001	.004	.005	.023

TABLE III - A

ELECTRICAL CHARACTERISTICS OF THE MO17 PHOTOSENSOR

ARRAY IN FLIGHT CAMERA 1B

Channel	Preamp Ser. No.	R_f, MΩ	R_i, Ω	Channel gain	r_a, μm	Diode noise, fA/$\sqrt{Hz}$	Preamp noise, fA/$\sqrt{Hz}$	Total noise, fA/$\sqrt{Hz}$
BB1	476	723.5	5,178	19.31	19.4	5.98	4.97	7.78
BB2	481	699.7	5,680	17.61	20.3	6.25	5.09	8.07
BB3	534	724.9	5,958	16.78	19.7	6.06	4.80	7.74
BB4	459	740.8	6,480	15.43	19.4	5.98	5.25	7.97
BB4	384	756.8	54,540	1.83	58.8	18.09	4.96	18.76
SURVEY	307	735.0	4,392	22.77	59.4	4.97	4.58	6.77
BLUE	301	709.5	4,082	24.50	58.8	4.64	5.07	6.89
GREEN	311	764.1	14,240	7.02	59.1	8.77	4.81	10.01
RED	305	719.5	7,064	14.16	58.2	6.14	4.98	7.92
IR1	317	707.1	4,561	21.93	58.8	5.18	5.17	7.33
IR2	303	752.2	6,037	16.56	58.8	5.75	4.83	7.52

TABLE III – B

ELECTRICAL CHARACTERISTICS OF THE MO20 PHOTOSENSOR

ARRAY IN FLIGHT CAMERA 2A

Channel	Preamp Ser.No.	R_f, MΩ	R_i, Ω	Channel gain	r_{a}, μm	Diode noise, fA/$\sqrt{Hz}$	Preamp noise, fA/$\sqrt{Hz}$	Total noise, fA/$\sqrt{Hz}$
BB1	454	712.5	6,133	16.31	21.3	6.56	5.13	8.34
BB2	353	674.6	4,147	24.11	18.4	5.66	5.19	7.69
BB3	477	753.3	6,597	15.16	21.0	6.45	4.75	8.02
BB4	536	747.9	6,523	15.33	21.0	6.45	4.78	8.04
SURVEY	462	740.3	55,678	1.80	59.7	18.36	5.04	19.04
BLUE	467	702.1	3,345	29.90	58.8	4.92	5.04	7.05
GREEN	658	649.3	3,654	27.37	59.1	4.66	4.92	6.79
RED	579	692.9	13,126	7.62	59.7	8.84	5.16	10.26
IR1	583	665.0	6,451	15.50	59.7	6.31	5.21	8.19
IR2	593	674.1	4,496	22.24	59.7	5.26	5.03	7.29
IR3	453	729.8	5,919	16.89	59.1	5.80	5.27	7.83

TABLE III – C

ELECTRICAL CHARACTERISTICS OF THE MO15 PHOTOSENSOR ARRAY IN FLIGHT CAMERA 3A

Channel	Preamp Ser.No.	R_f MΩ	R_i Ω	Channel gain	r_a, μm	Diode noise, fA/$\sqrt{Hz}$	Preamp noise, fA/$\sqrt{Hz}$	Total noise, fA/$\sqrt{Hz}$
BB1	640	730.4	5,026	19.9	20.7	6.37	4.95	8.08
BB2	581	740.4	5,620	17.8	20.3	6.25	4.73	7.85
BB3	350	742.9	6,201	16.1	20.7	6.37	5.07	8.15
BB4	621	672.8	4,697	21.3	20.1	6.17	4.86	7.87
SURVEY	292	728.1	51,615	1.94	58.8	18.1	5.53	18.9
BLUE	667	703.5	3,400	29.4	58.8	4.98	4.92	6.97
GREEN	240	741.4	3,900	25.6	58.8	4.64	5.33	7.08
RED	224	712.1	13,527	7.39	58.8	8.73	5.01	10.1
IR1	615	667.8	6,684	15.0	59.7	6.54	5.42	8.58
IR2	420	762.2	5,393	18.5	59.4	5.40	4.70	7.17
IR3	660	732.5	6,139	16.3	59.4	5.99	4.68	7.61

TABLE III - D

ELECTRICAL CHARACTERISTICS OF THE MO19 PHOTOSENSOR

ARRAY IN FLIGHT CAMERA SPARE

Channel	Preamp Ser.No.	R_f, MΩ	R_i, Ω	Channel gain	r_a, μm	Diode noise, fA/$\sqrt{Hz}$	Preamp noise, fA/$\sqrt{Hz}$	Total noise, fA/$\sqrt{Hz}$
BB1	490	730.9	8,108	12.33	22.0	6.76	5.03	8.43
BB2	392	731.8	7,387	13.54	21.0	6.45	4.92	8.12
BB3	474	743.9	6,626	15.09	19.7	6.06	5.17	7.97
BB4	542	715.8	7,535	13.27	21.3	6.56	4.71	8.09
SURVEY	333	727.8	60,314	1.66	58.8	18.09	5.04	18.78
BLUE	546	654.4	3,919	25.52	59.4	4.97	4.97	7.04
GREEN	527	719.1	3,836	26.07	59.4	4.69	4.92	6.81
RED	458	735.9	13,757	7.27	59.4	8.83	4.86	10.08
IR1	564	684.4	6,333	15.79	58.4	6.17	5.17	8.06
IR2	302	696.8	4,526	22.09	58.8	5.18	5.13	7.30
IR3	529	662.2	5,199	19.23	58.4	5.72	4.96	7.58

TABLE IV

GAIN AND OFFSET CALIBRATION CONSTANTS

Flight Camera	Calibration constants		
	k_g	k_{co}	k_o
1B	444.321	0.14410	0.204
2A	442.135	0.14469	0.209
3A	447.634	0.14583	0.222
Spare	448.111	0.14389	0.217

TABLE V

GREY PATCH REFLECTANCES AND

CALIBRATION FIXTURE CORRECTIONS

n	ρ_n	c_n
1	.095	1.085
2	.130	1.040
3	.196	1.031
4	.245	1.181
5	.308	1.238
6	.356	1.029
7	.400	.949
8	.458	1.000
9	.527	1.034
10	.572	1.085
11	.762	1.142
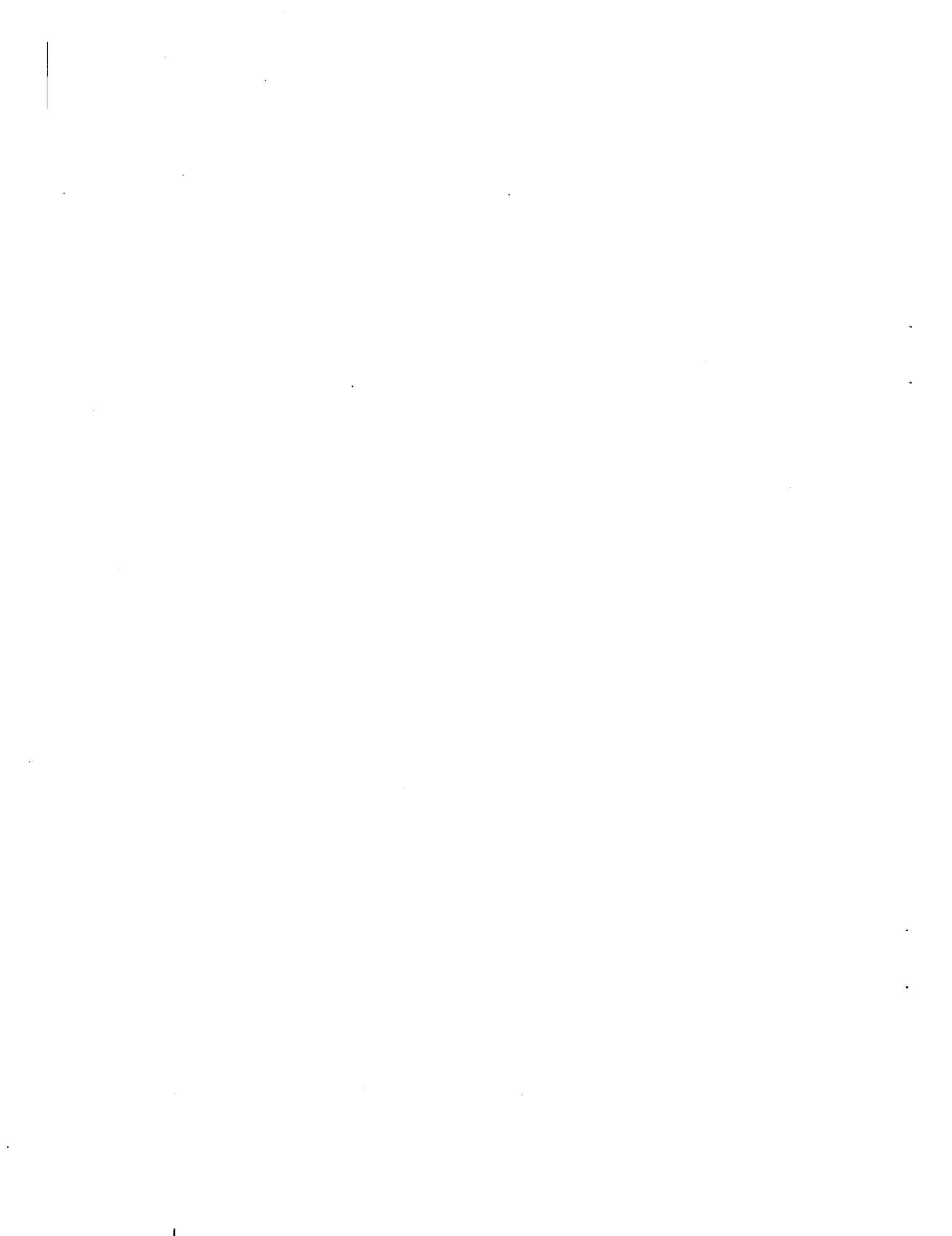
TABLE VI

NBS LAMP IRRADIANCE AT 50 CM

λ, μm	Irradiance, mW-cm^{-2}-μm^{-1}		
	EPI-1569	EPI-1568	EPI-1574
.30	.193	.200	.180
.32	.366	.382	.343
.35	.826	.856	.777
.37	1.28	1.35	1.21
.40	2.23	2.26	2.11
.45	4.48	4.61	4.31
.50	7.52	7.67	7.18
.55	11.0	11.2	10.5
.60	14.6	14.8	14.0
.65	18.0	18.2	17.2
.70	20.9	21.1	19.9
.75	23.2	23.4	22.0
.80	24.7	25.0	23.6
.90	25.5	25.7	24.8
1.0	24.8	25.1	24.0
1.1	23.5	23.8	22.5

EPI - 1569 lamp was used in Itek tests

EPI - 1568 lamp was used in initial Denver tests and for predictions

EPI - 1574 lamp was used in later Denver and Cape Kennedy tests

TABLE VII-A

RADIOMETRIC CALIBRATION DATA FOR FLIGHT CAMERA 1B

Camera Channel	Gain	Offset	Reference test chart grey patch
			1	2	3	4	5	6	7	8	9	10	11
---	---	---	---	---	---	---	---	---	---	---	---	---	---
BB1	4	2	4.26	7.60	12.06	15.00	18.89	26.93	31.33	35.93	37.53	42.03	53.32
BB2	4	2	4.12	7.21	12.02	14.98	18.83	26.93	31.08	36.05	37.48	42.13	53.24
BB3	4	2	5.00	7.97	12.58	15.30	19.34	27.98	32.26	37.39	38.98	43.65	54.63
BB4	4	2	4.14	7.58	12.02	14.93	18.68	26.55	30.96	35.79	36.98	41.60	52.15
SURVEY	4	2	4.99	8.00	12.99	15.61	19.61	28.00	32.24	37.71	38.90	43.31	54.32
BLUE	3	2	3.03	6.35	10.92	13.67	17.14	25.99	30.37	34.88	36.43	41.06	51.07
GREEN	3	2	4.87	9.12	14.93	18.37	23.23	33.48	39.02	44.61	46.79	52.79	62.00
RED	3	2	5.32	10.00	16.82	20.98	26.50	38.65	44.82	51.83	54.57	61.59	62.00
IR1	4	4	0.00	3.72	10.47	14.00	19.90	31.10	38.02	45.12	46.28	52.61	62.00
IR2	4	5	0.00	2.40	10.87	15.23	22.22	35.58	43.97	52.46	53.90	61.40	62.00
IR3	4	6	0.00	0.00	7.12	11.78	18.65	32.16	40.97	49.16	50.60	58.43	62.00

Obtained at MMC, 9/20/74

TABLE VII-B

RADIOMETRIC CALIBRATION DATA FOR FLIGHT CAMERA 2A

Camera Channel	Gain	Offset	Reference test chart grey patch										
			1	2	3	4	5	6	7	8	9	10	11
BB1	4	2	4.67	7.84	12.02	14.96	18.70	26.78	31.00	35.64	37.13	41.50	52.72
BB2	4	2	4.22	7.24	11.95	14.63	18.27	26.71	31.05	35.67	37.06	41.77	52.53
BB3	4	2	4.41	7.15	11.99	14.89	18.48	26.94	31.00	35.85	37.31	41.77	52.74
BB4	4	2	4.66	7.98	12.35	15.02	19.12	27.67	32.00	37.12	38.68	43.04	54.37
SURVEY	4	2	4.85	8.00	12.91	15.34	19.00	27.79	32.01	37.13	38.50	42.98	54.63
BLUE	3	2	5.75	9.68	15.55	18.98	23.35	34.16	39.50	45.31	47.37	53.05	62.00
GREEN	3	2	5.12	9.40	15.31	18.94	23.81	35.28	41.21	47.26	49.09	55.16	62.00
RED	3	2	5.23	9.98	16.27	20.49	25.95	38.12	44.01	51.66	53.88	60.72	62.00
IR1	4	4	0.00	4.43	11.43	15.24	21.07	33.57	40.84	47.56	49.35	55.49	62.00
IR2	4	5	0.00	2.44	11.03	15.12	21.99	35.61	43.51	52.35	54.07	61.48	62.00
IR3	4	6	0.00	0.03	9.26	14.08	21.58	36.76	45.56	55.19	56.71	62.00	62.00

Obtained at MMC, 9/19/74

TABLE VII-C

RADIOMETRIC CALIBRATION DATA FOR FLIGHT CAMERA 3A

Channel	Camera Gain	Offset	Reference test chart grey patch										
			1	2	3	4	5	6	7	8	9	10	11
BB1	4	2	4.99	7.21	13.28	17.09	21.76	28.07	34.89	39.33	41.92	47.58	60.00
BB2	4	2	5.00	7.26	13.88	17.69	22.32	28.52	35.45	40.22	47.82	48.85	61.00
BB3	4	2	5.31	8.21	15.39	18.13	22.61	28.89	37.28	43.79	43.93	49.25	52.00
BB4	4	2	5.06	9.10	15.82	18.24	22.13	29.39	37.55	43.91	43.22	48.34	61.30
SURVEY	4	2	5.93	8.00	14.96	18.81	23.69	30.88	38.64	43.17	45.67	51.15	62.00
BLUE	3	2	4.93	8.02	15.37	19.61	24.45	31.80	39.84	44.64	48.13	54.37	62.00
GREEN	3	2	5.92	9.47	18.31	23.45	29.24	37.31	46.71	52.79	57.21	62.00	62.00
RED	3	2	4.98	8.00	16.22	21.26	27.14	35.06	44.08	50.30	54.28	61.42	62.00
IR1	4	2	7.05	10.10	18.97	24.00	30.09	39.43	49.36	55.28	58.34	62.00	62.00
IR2	4	2	9.00	12.38	22.97	28.86	36.41	46.75	58.73	62.00	62.00	62.00	62.00
IR3	4	2	10.56	14.93	27.01	33.49	42.31	53.81	62.00	62.00	62.00	62.00	62.00

Obtained at MMC, 10/9/74

TABLE VII-D

RADIOMETRIC CALIBRATION DATA FOR FLIGHT CAMERA SPARE

Camera Channel	Gain	Offset	Reference test chart grey patch										
			1	2	3	4	5	6	7	8	9	10	11
BB1	4	2	4.42	7.60	12.02	14.99	18.44	26.88	31.19	35.22	36.80	41.42	52.26
BB2	4	2	4.14	7.21	12.00	14.98	18.57	27.03	31.63	35.58	37.05	41.75	52.56
BB3	4	2	5.00	7.88	12.51	15.33	18.98	27.52	32.00	36.34	37.83	42.29	53.38
BB4	4	2	4.51	7.94	12.45	15.02	19.01	27.81	32.14	36.64	38.33	42.74	53.94
SURVEY	4	2	4.72	7.98	12.91	15.00	18.98	27.64	32.26	36.27	37.77	42.36	53.43
BLUE	3	2	4.63	7.93	13.14	16.05	19.90	29.88	34.77	38.99	40.82	45.93	56.98
GREEN	3	2	5.09	9.14	14.97	18.27	22.75	33.90	39.50	45.02	46.36	52.22	62.00
RED	3	2	5.09	9.98	16.27	20.14	25.55	38.28	44.67	50.93	53.04	59.79	62.00
IR1	4	4	0.00	2.31	8.66	11.94	16.65	27.92	34.58	39.21	40.79	45.83	60.33
IR2	4	5	0.00	1.57	10.45	14.05	20.25	34.10	41.72	49.46	50.69	57.70	62.00
IR3	4	6	0.00	0.04	9.59	13.99	21.07	36.60	45.45	54.27	55.21	62.00	62.00

Obtained at MMC, 11/15/74

TABLE VIII - A

COMPARISON OF PERFORMANCE PREDICTIONS AND CALIBRATION MEASUREMENTS FOR FLIGHT CAMERA 1B.

GIVEN ARE THE RATIOS OF MEASUREMENT OVER PREDICTION(IN VOLTS) AT THE PHOTOSENSOR ARRAY OUTPUT.

ρ	c_n	BB1	BB2	BB3	BB4	Photosensor array channels Survey	Blue	Green	Red	IR1	IR2	IR3
.095	1.085	0.251/0.233=1.08	0.245/0.234=1.05	0.280/0.243=1.15	0.246/0.229=1.07	0.279/0.244=1.14	0.143/0.107=1.34	0.179/0.130=1.38	0.188/0.189=1.0	0.512/0.490=1.05	0.606/0.507=1.20	
.130	1.040	0.369/0.318=1.16	0.354/0.320=1.11	0.38?/0.352=1.11	0.368/0.314=1.17	0.384/0.333=1.15	0.202/0.148=1.29	0.255/0.178=1.43	0.271/0.256=1.05	0.761/0.739=1.03	0.920/0.765=1.20	0.925/0.714=1.24
.196	1.031	0.532/0.480=1.11	0.530/0.482=1.10	0.551/0.500=1.10	0.530/0.473=1.13	0.566/0.503=1.13	0.257/0.221=1.30	0.261/0.269=1.34	0.296/0.289=1.02	0.968/0.924=1.05	1.164/0.956=1.22	1.162/0.930=1.25
.245	1.161	0.722/0.600=1.20	0.721/0.602=1.20	0.735/0.625=1.18	0.719/0.592=1.21	0.748/0.628=1.19	0.375/0.276=1.36	0.475/0.339=1.41	0.530/0.467=1.09	1.260/1.162=1.10	1.507/1.202=1.25	1.492/1.169=1.25
.308	1.238	0.926/0.754=1.23	0.924/0.757=1.22	0.946/0.786=1.20	0.917/0.744=1.23	0.958/0.790=1.21	0.466/0.347=1.34	0.602/0.422=1.45	0.675/0.612=1.10	1.525/1.343=1.13	1.835/1.390=1.32	1.852/1.352=1.37
.356	1.029	1.082/0.872=1.24	1.082/0.875=1.24	1.121/0.909=1.23	1.068/0.859=1.24	1.22/0.913=1.23	0.566/0.401=1.41	0.704/0.488=1.41	0.800/0.707=1.13	1.672/1.505=1.11	2.019/1.557=1.30	2.061/1.515=1.36
.400	0.949	1.155/0.977=1.18	1.146/0.981=1.17	1.187/1.018=1.17	1.142/0.963=1.19	1.186/1.023=1.16	0.603/0.419=1.34	0.751/0.547=1.35	0.650/0.793=1.07	1.997/1.728=1.12	2.406/1.788=1.35	2.431/1.739=1.40
.458	1.000	1.378/1.122=1.23	1.382/1.126=1.23	1.431/1.169=1.22	1.373/1.106=1.24	1.442/1.175=1.23	0.712/0.516=1.38	0.887/0.628=1.41	1.017/0.910=1.12	2.096/1.988=1.05	2.523/2.057=1.23	2.545/2.001=1.27
.527	1.034	1.462/1.291=1.15	1.480/1.296=1.14	1.536/1.345=1.14	1.461/1.272=1.15	1.533/1.352=1.13	0.762/0.593=1.28	0.955/0.723=1.32	1.100/1.047=1.05	2.428/2.158=1.13		
.572	1.085	1.726/1.401=1.23	1.730/1.406=1.23	1.790/1.460=1.23	1.710/1.381=1.24	1.776/1.467=1.21	0.366/0.244=1.44	1.115/0.791=1.42				2.944/2.172=1.36
.762	1.142	2.277/1.866=1.22	2.274/1.873=1.21	2.331/1.945=1.20	2.229/1.840=1.21	2.339/1.954=1.20	1.134/0.858=1.32					
Average ratio, k_c		1.18	1.17	1.17	1.18	1.19	1.18	1.35	1.39	1.07	1.09	1.32

TABLE VIII - B

COMPARISON OF PERFORMANCE PREDICTIONS AND CALIBRATION MEASUREMENTS FOR FLIGHT CAMERA 2A.
GIVEN ARE THE RATIOS OF MEASUREMENT OVER PREDICTION(IN VOLTS) AT THE PHOTOSENSOR ARRAY OUTPUT.

ρ	c_n	Photosensor array channels										
		BB1	BB2	BB3	BB4	Survey	Blue	Green	Red	IR1	IR2	IR3
.095	1.085	0.264/0.231 =1.14	0.246/0.234 =1.05	0.254/0.226 =1.12	0.263/0.239 =1.10	0.271/0.240 =1.13	0.193/0.134 =1.44	0.181/0.127 =1.42	0.183/0.185 =0.99			
.130	1.040	0.375/0.316 =1.19	0.353/0.320 =1.10	0.349/0.309 =1.13	0.381/0.328 =1.16	0.381/0.329 =1.16	0.263/0.184 =1.43	0.257/0.174 =1.48	0.268/0.254 =1.06	0.536/0.517 =1.04	0.606/0.508 =1.19	
.196	1.031	0.529/0.477 =1.11	0.526/0.483 =1.09	0.528/0.466 =1.13	0.541/0.494 =1.10	0.562/0.495 =1.14	0.370/0.277 =1.34	0.366/0.263 =1.39	0.384/0.382 =1.01	0.796/0.780 =1.02	0.926/0.766 =1.21	1.005/0.776 =1.30
.245	1.181	0.720/0.596 =1.21	0.706/0.603 =1.17	0.717/0.583 =1.23	0.722/0.618 =1.17	0.726/0.619 =1.17	0.486/0.347 =1.40	0.465/0.329 =1.47	0.518/0.477 =1.09	1.021/0.975 =1.05	1.161/0.958 =1.21	1.261/0.970 =1.30
.308	1.238	0.918/0.749 =1.23	0.899/0.758 =1.19	0.908/0.732 =1.24	0.937/0.776 =1.21	0.932/0.778 =1.20	0.603/0.436 =1.38	0.614/0.413 =1.49	0.662/0.601 =1.10	1.314/1.226 =1.07	1.500/1.204 =1.25	1.626/1.219 =1.33
.356	1.029	1.078/0.866 =1.24	1.075/0.877 =1.23	1.084/0.846 =1.28	1.111/0.897 =1.24	1.115/0.900 =1.24	0.716/0.504 =1.42	0.737/0.477 =1.55	0.790/0.694 =1.14	1.620/1.417 =1.14	1.840/1.391 =1.32	2.068/1.409 =1.44
.400	0.949	1.145/0.970 =1.18	1.147/0.963 =1.17	1.145/0.949 =1.21	1.179/1.006 =1.17	1.180/1.008 =1.17	0.759/0.565 =1.34	0.788/0.535 =1.47	0.836/0.779 =1.07	1.772/1.588 =1.12	2.009/1.560 =1.29	2.224/1.580 =1.41
.458	1.000	1.370/1.114 =1.23	1.371/1.128 =1.22	1.378/1.089 =1.27	1.424/1.154 =1.23	1.424/1.157 =1.23	0.900/0.648 =1.39	0.936/0.611 =1.52	1.015/0.893 =1.14	2.091/1.823 =1.15	2.409/1.790 =1.35	2.656/1.813 =1.46
.527	1.034	1.470/1.281 =1.15	1.467/1.298 =1.13	1.476/1.253 =1.18	1.528/1.328 =1.15	1.521/1.332 =1.14	0.967/0.746 =1.30	0.999/0.707 =1.41	1.088/1.028 =1.06	2.216/2.097 =1.06	2.538/2.060 =1.23	2.781/2.086 =1.33
.572	1.085	1.714/1.391 =1.23	1.720/1.408 =1.22	1.720/1.360 =1.26	1.770/1.442 =1.23	1.768/1.445 =1.22	1.122/0.879 =1.28	1.163/0.790 =1.47	1.272/1.115 =1.14	2.549/2.276 =1.12		
.762	1.142	2.252/1.853 =1.22	2.251/1.876 =1.20	2.260/1.812 =1.25	2.327/1.921 =1.21	2.338/1.926 =1.21						
Average ratio, k_c		1.19	1.16	1.21	1.18	1.18	1.38	1.47	1.08	1.09	1.26	1.37

TABLE VIII - C

COMPARISON OF PERFORMANCE PREDICTIONS AND CALIBRATION MEASUREMENTS FOR FLIGHT CAMERA 3A.

GIVEN ARE THE RATIOS OF MEASUREMENT OVER PREDICTION(IN VOLTS) AT THE PHOTOSENSOR ARRAY OUTPUT.

ρ	c_n	BB1	BB2	BB3	BB4	Survey	Blue	Green	Red	IR1	IR2	IR3
.095	1.085	$\frac{0.263}{0.226}$=1.16	$\frac{0.264}{0.232}$=1.11	$\frac{0.276}{0.238}$=1.16	$\frac{0.266}{0.240}$=1.11	$\frac{0.300}{0.250}$=1.20	$\frac{0.165}{0.115}$=1.42	$\frac{0.184}{0.138}$=1.33	$\frac{0.166}{0.15?}$=1.08	$\frac{0.243}{0.22?}$=1.07	$\frac{0.419}{0.345}$=1.21	$\frac{0.472}{0.345}$=1.24
.139	1.040	$\frac{0.338}{0.310}$=1.09	$\frac{0.340}{0.318}$=1.07	$\frac{0.375}{0.325}$=1.15	$\frac{0.408}{0.329}$=1.24	$\frac{0.367}{0.343}$=1.07	$\frac{0.219}{0.199}$	$\frac{0.246}{0.188}$	$\frac{0.218}{0.220}$=1.01	$\frac{0.445}{0.440}$=1.01	$\frac{0.530}{0.471}$=1.13	$\frac{0.625}{0.527}$=1.19
.196	1.031	$\frac{0.559}{0.467}$=1.20	$\frac{0.581}{0.479}$=1.21	$\frac{0.637}{0.490}$=1.30	$\frac{0.653}{0.496}$=1.32	$\frac{0.621}{0.517}$=1.20	$\frac{0.352}{0.239}$	$\frac{0.407}{0.284}$=1.43	$\frac{0.369}{0.317}$=1.16	$\frac{0.769}{0.663}$=1.16	$\frac{0.916}{0.711}$=1.29	$\frac{1.055}{0.795}$=1.34
.245	1.181	$\frac{0.791}{0.583}$=1.36	$\frac{0.816}{0.599}$=1.36	$\frac{0.835}{0.613}$=1.36	$\frac{0.840}{0.620}$=1.35	$\frac{0.864}{0.646}$=1.34	$\frac{0.484}{0.299}$=1.62	$\frac{0.565}{0.355}$=1.59	$\frac{0.518}{0.396}$=1.31	$\frac{1.083}{0.829}$=1.31	$\frac{1.288}{0.889}$=1.45	$\frac{1.483}{0.994}$=1.49
.308	1.238	$\frac{1.033}{0.733}$=1.41	$\frac{1.057}{0.752}$=1.41	$\frac{1.070}{0.770}$=1.39	$\frac{1.049}{0.779}$=1.35	$\frac{1.118}{0.812}$=1.38	$\frac{0.611}{0.376}$=1.63	$\frac{0.717}{0.446}$=1.61	$\frac{0.670}{0.498}$=1.35	$\frac{1.401}{1.042}$=1.34	$\frac{1.681}{1.117}$=1.50	$\frac{1.942}{1.250}$=1.55
.356	1.029	$\frac{1.102}{0.847}$=1.30	$\frac{1.119}{0.870}$=1.29	$\frac{1.132}{0.890}$=1.27	$\frac{1.151}{0.900}$=1.28	$\frac{1.205}{0.938}$=1.28	$\frac{0.654}{0.434}$=1.51	$\frac{0.756}{0.515}$=1.47	$\frac{0.714}{0.576}$=1.24	$\frac{1.520}{1.205}$=1.26	$\frac{1.789}{1.291}$=1.39	$\frac{2.049}{1.444}$=1.42
.400	0.949	$\frac{1.253}{0.950}$=1.32	$\frac{1.272}{0.975}$=1.30	$\frac{1.334}{0.998}$=1.34	$\frac{1.343}{1.009}$=1.33	$\frac{1.380}{1.052}$=1.31	$\frac{0.745}{0.487}$=1.53	$\frac{0.862}{0.578}$=1.49	$\frac{0.817}{0.645}$=1.27	$\frac{1.744}{1.350}$=1.29	$\frac{2.062}{1.447}$=1.43	
.458	1.000	$\frac{1.475}{1.090}$=1.35	$\frac{1.507}{1.119}$=1.35	$\frac{1.490}{1.146}$=1.30	$\frac{1.494}{1.158}$=1.29	$\frac{1.613}{1.207}$=1.34	$\frac{0.867}{0.559}$=1.55	$\frac{1.013}{0.663}$=1.53	$\frac{0.969}{0.740}$=1.31	$\frac{2.046}{1.550}$=1.32		
.527	1.034	$\frac{1.619}{1.255}$=1.29	$\frac{1.652}{1.288}$=1.29	$\frac{1.692}{1.318}$=1.28	$\frac{1.667}{1.333}$=1.25	$\frac{1.758}{1.389}$=1.27	$\frac{0.952}{0.643}$=1.49	$\frac{1.127}{0.763}$=1.49	$\frac{1.073}{0.852}$=1.26	$\frac{2.226}{1.784}$=1.25		
.572	1.085	$\frac{1.915}{1.362}$=1.41	$\frac{1.965}{1.397}$=1.41	$\frac{1.980}{1.431}$=1.38	$\frac{1.944}{1.446}$=1.34	$\frac{2.053}{1.507}$=1.36	$\frac{1.124}{0.698}$=1.61					
.762	1.145	$\frac{2.557}{1.814}$=1.41										
Average ratio, k_c	1.30	1.28	1.28	1.29	1.28	1.28	1.52	1.47	1.22	1.22	1.34	1.37

TABLE VIII - D

COMPARISON OF PERFORMANCE PREDICTIONS AND CALIBRATION MEASUREMENTS FOR FLIGHT CAMERA SPARE

GIVEN ARE THE RATIOS OF MEASUREMENTS OVER PREDICTIONS(IN VOLTS) AT THE PHOTOSENSOR ARRAY OUTPUT.

ρ	c_n	BB1	BB2	BB3	BB4	Survey	Blue	Green	Red	IR1	IR2	IR3
.095	1.085	0.242/0.233 =1.04	0.231/0.240 =0.96	0.264/0.238 =1.11	0.245/0.243 =1.01	0.254/0.242 =1.05	0.160/0.120 =1.33	0.169/0.130 =1.30	0.169/0.188 =0.90			
.130	1.040	0.353/0.319 =1.11	0.339/0.328 =1.03	0.363/0.325 =1.12	0.366/0.332 =1.10	0.367/0.331 =1.11	0.218/0.164 =1.33	0.240/0.178 =1.33	0.256/0.258 =0.99	0.444/0.455 =0.98	0.561/0.504 =1.11	
.196	1.031	0.513/0.480 =1.07	0.513/0.494 =1.04	0.531/0.491 =1.08	0.529/0.501 =1.06	0.546/0.499 =1.09	0.313/0.245 =1.26	0.346/0.270 =1.28	0.370/0.388 =0.95	0.677/0.686 =0.99	0.887/0.759 =1.17	0.999/0.782 =1.28
.245	1.181	0.703/0.600 =1.17	0.702/0.618 =1.14	0.717/0.613 =1.17	0.704/0.626 =1.13	0.703/0.624 =1.13	0.409/0.310 =1.32	0.456/0.336 =1.36	0.495/0.485 =1.02	0.862/0.858 =1.01	1.095/0.949 =1.15	1.236/0.978 =1.26
.308	1.238	0.886/0.755 =1.17	0.892/0.777 =1.15	0.910/0.771 =1.18	0.911/0.787 =1.16	0.910/0.784 =1.16	0.511/0.389 =1.31	0.574/0.423 =1.36	0.635/0.610 =1.04	1.055/1.079 =1.02	1.398/1.193 =1.17	1.578/1.229 =1.28
.356	1.029	1.058/0.872 =1.21	1.064/0.898 =1.19	1.082/0.891 =1.21	1.093/0.909 =1.20	1.086/0.906 =1.20	0.620/0.450 =1.38	0.694/0.488 =1.42	0.774/0.705 =1.10	1.284/1.247 =1.11	1.755/1.379 =1.27	1.991/1.421 =1.40
.400	0.949	1.128/0.978 =1.15	1.143/1.006 =1.14	1.155/0.999 =1.16	1.160/1.019 =1.14	1.164/1.015 =1.15	0.660/0.504 =1.31	0.740/0.547 =1.35	0.828/0.791 =1.05	1.530/1.397 =1.10	1.916/1.546 =1.24	2.186/1.592 =1.37
.458	1.000	1.328/1.122 =1.18	1.341/1.155 =1.16	1.368/1.176 =1.16	1.379/1.170 =1.18	1.365/1.166 =1.17	0.767/0.579 =1.33	0.877/0.628 =1.39	0.980/0.908 =1.08	1.759/1.601 =1.10	2.268/1.775 =1.28	2.584/1.828 =1.41
.527	1.034	1.429/1.291 =1.11	1.439/1.329 =1.08	1.467/1.319 =1.11	1.486/1.346 =1.10	1.465/1.341 =1.09	0.824/0.606 =1.24	0.927/0.723 =1.28	1.050/1.044 =1.01	1.865/1.846 =1.01	2.374/2.042 =1.16	2.685/2.103 =1.28
.572	1.085	1.675/1.401 =1.20	1.688/1.442 =1.17	1.709/1.432 =1.19	1.727/1.461 =1.18	1.751/1.456 =1.20	0.960/0.723 =1.33	1.082/0.785 =1.38	1.229/1.133 =1.09	2.134/2.003 =1.07	2.738/2.216 =1.24	
.762	1.142	2.202/1.867 =1.18	2.214/1.910 =1.16	2.247/1.907 =1.18	2.270/1.946 =1.17	2.249/1.940 =1.16	1.232/0.963 =1.28			2.810/2.669			
Average ratio,k_c		1.14	1.11	1.16	1.13	1.14	1.31	1.35	1.02	1.04	1.20	1.33

TABLE VIII - E

SUMMARY OF PHOTOSENSOR ARRAY CALIBRATION FACTORS k_c.

Camera	BB1	BB2	BB3	BB4	Survey	Blue	Green	Red	IR1	IR2	IR3
					Photosensor array channel						
1B	1.18	1.17	1.18	1.19	1.18	1.35	1.39	1.07	1.09	1.26	1.32
2A	1.19	1.16	1.21	1.18	1.18	1.38	1.47	1.08	1.09	1.26	1.57
3A	1.30	1.28	1.29	1.28	1.28	1.52	1.47	1.22	1.22	1.34	1.37
Spare	1.14	1.11	1.16	1.13	1.14	1.31	1.35	1.02	1.04	1.20	1.33

TABLE IV

AVERAGE MARS RADIANCE DATA AT 1.6 A.U.

λ, μm	$S(\lambda)$, kW/m^2-μm	$\tau(\lambda;1_o)$	$\rho_m(\lambda)$	$N(\lambda)$, kW/m^2-sr-μm
.300	.238	.682	.029	.0015
.325	.398	.748	.036	.0034
.350	.461	.820	.043	.0051
.375	.516	.854	.051	.0071
.400	.602	.890	.058	.0100
.425	.738	.906	.066	.0141
.450	.859	.921	.074	.0187
.475	.859	.938	.083	.0214
.500	.773	.954	.092	.0217
.525	.750	.960	.106	.0242
.550	.762	.965	.119	.0279
.575	.731	.971	.133	.0300
.600	.707	.977	.146	.0322
.625	.672	.979	.163	.0342
.650	.633	.981	.180	.0356
.675	.598	.983	.197	.0368
.700	.562	.985	.214	.0377
.725	.529	.987	.219	.0365
.750	.496	.989	.225	.0351
.775	.469	.991	.225	.0333
.800	.441	.992	.225	.0314
.825	.416	.992	.224	.0294
.850	.391	.992	.223	.0275
.875	.370	.993	.223	.0260
.900	.349	.993	.223	.0246
.925	.332	.993	.219	.0230
.950	.314	.993	.216	.0214
.975	.298	.993	.215	.0203
1.000	.283	.993	.214	.0191
1.025	.276	.993	.213	.0182
1.050	.260	.993	.212	.0174
1.075	.248	.993	.214	.0168
1.100	.237	.993	.217	.0162

TABLE X

PHOTOSENSOR ARRAY OUTPUT SIGNALS (VOLTS) FOR A 40% REFLECTANCE GREY PATCH AND A SUN INCIDENCE ANGLE OF 60°.

Camera	Photosensor array channel										
	BB1	BB2	BB3	BB4	Survey	Blue	Green	Red	IR1	IR2	IR3
1B	1.65	1.63	1.70	1.63	1.68	2.94	2.57	1.39	1.29	1.47	1.59
2A	1.65	1.63	1.61	1.70	1.62	3.85	2.71	1.37	1.36	1.48	1.69
3A	1.75	1.80	1.86	1.86	1.87	3.81	2.98	1.34	1.32	1.47	1.71
Spare	1.60	1.60	1.65	1.65	1.59	3.21	2.46	1.31	1.16	1.39	1.65
Average	1.66	1.66	1.71	1.71	1.69	3.45	2.68	1.35	1.28	1.45	1.66

TABLE XI

PHOTOSENSOR ARRAY OUTPUT SIGNALS (VOLTS)

FOR THE AVERAGE MARS RADIANCE AND THE ILLUMINATION SCATTERING FUNCTION EQUAL TO UNITY.

Camera	Photosensor array channel										
	BB1	BB2	BB3	BB4	Survey	Blue	Green	Red	IR1	IR2	IR3
1B	1.41	1.40	1.46	1.40	1.45	1.37	1.53	1.32	1.43	1.50	1.58
2A	1.41	1.39	1.39	1.45	1.41	1.78	1.60	1.30	1.51	1.51	1.68
3A	1.50	1.53	1.58	1.58	1.61	1.73	1.74	1.25	1.47	1.51	1.71
Spare	1.36	1.36	1.41	1.41	1.38	1.47	1.67	1.25	1.28	1.43	1.64
Average	1.42	1.42	1.46	1.46	1.46	1.59	1.58	1.28	1.42	1.49	1.65

TABLE XII

NOISE-EQUIVALENT RADIANCES (mW-m^{-2}-sr^{-1}) AT THE PHOTOSENSOR

ARRAY OUTPUT (PRIOR TO QUANTIZATION).

Scan rate	Camera	Photosensor array channel										
		BB1	BB2	BB3	BB4	Survey	Blue	Green	Red	IR1	IR2	IR3
Slow	1B	10	10	9	9	2.4	11	11	5.5	8	10	8
	2A	9	12	9	9	2.4	11	10	5.6	8	10	8
	3A	11	9	8	10	2.2	11	10	5.7	8	9	7
	Spare	8	8	9	7	2.2	11	12	5.8	9	11	8
	Average	10	10	9	9	2.3	11	11	5.7	8	10	8
Rapid	1B	74	68	62	63	17	79	75	39	54	73	57
	2A	66	86	63	61	17	80	73	40	54	70	55
	3A	75	65	59	69	16	80	74	41	56	64	51
	Spare	54	57	61	52	16	76	84	42	65	76	57
	Average	67	69	61	61	17	79	77	41	57	71	55

TABLE XIII

TYPICAL NOISE-EQUIVALENT RADIANCES ($W\text{-}m^{-2}\text{-}sr^{-1}$) FOR ALL GAINS AND SCAN RATES

Scan rate	Gain number	Hi-Res	Survey	Photosensor array channel					
				Blue	Green	Red	IR1	IR2	IR3
Slow	0	.013	.008	.014	.013	.010	.011	.013	.011
	1	.019	.016	.020	.019	.018	.018	.019	.017
	2	.035	.032	.036	.032	.035	.033	.033	.030
	3	.067	.064	.068	.062	.070	.065	.063	.059
	4	.133	.128	.135	.122	.141	.130	.124	.118
	5	.265	.256	.270	.243	.281	.259	.247	.235
Rapid	0	.069	.019	.080	.076	.040	.055	.073	.058
	1	.070	.024	.081	.077	.043	.056	.074	.059
	2	.076	.036	.086	.081	.053	.063	.079	.064
	3	.095	.066	.104	.097	.080	.084	.095	.082
	4	.149	.129	.156	.143	.146	.140	.143	.131
	5	.274	.257	.281	.254	.284	.264	.257	.242

TABLE XIV

TYPICAL SIGNAL-TO-NOISE RATIOS FOR ALL GAINS AND SCAN RATES

Scan rate	Gain number	Photosensor array channel							
		Hi-Res	Survey	Blue	Green	Red	IR1	IR2	IR3
Slow	0	1433	2169	1302	1398	1754	1638	1422	1673
	1	948	1120	899	983	987	1016	982	1085
	2	526	565	511	565	511	546	559	596
	3	271	283	265	295	258	279	290	306
	4	137	142	134	149	129	140	147	154
	5	68	71	67	75	65	70	74	77
Rapid	0	264	955	228	276	453	332	249	316
	1	258	771	224	272	424	322	245	308
	2	240	499	211	258	346	288	230	283
	3	191	273	174	216	226	215	191	222
	4	122	140	116	146	125	129	127	139
	5	66	71	65	82	69	67	71	75
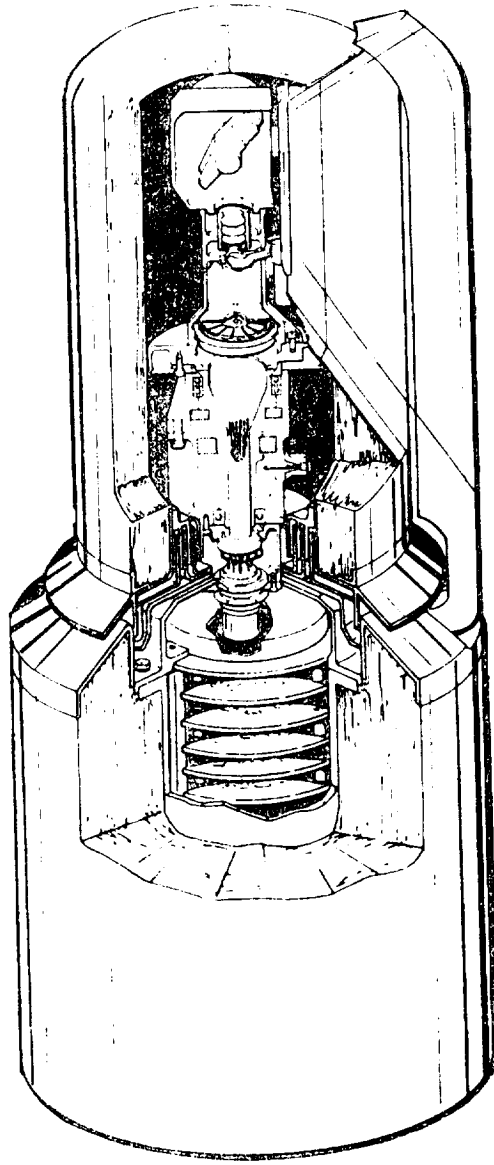
Figure 1.- Simplified cutaway view of the Viking lander camera.
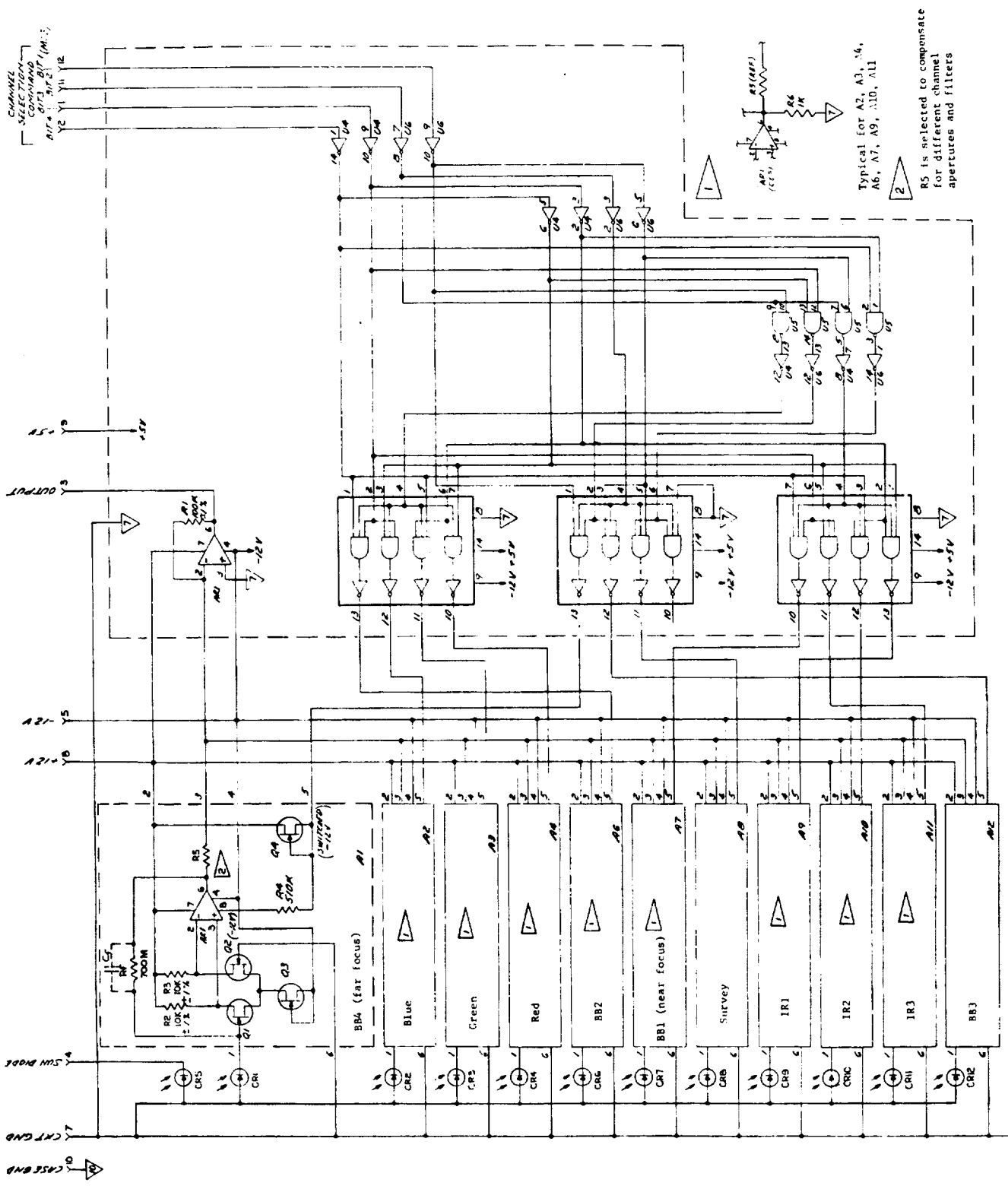
Figure 2.– Circuit diagram of the photosensor array.
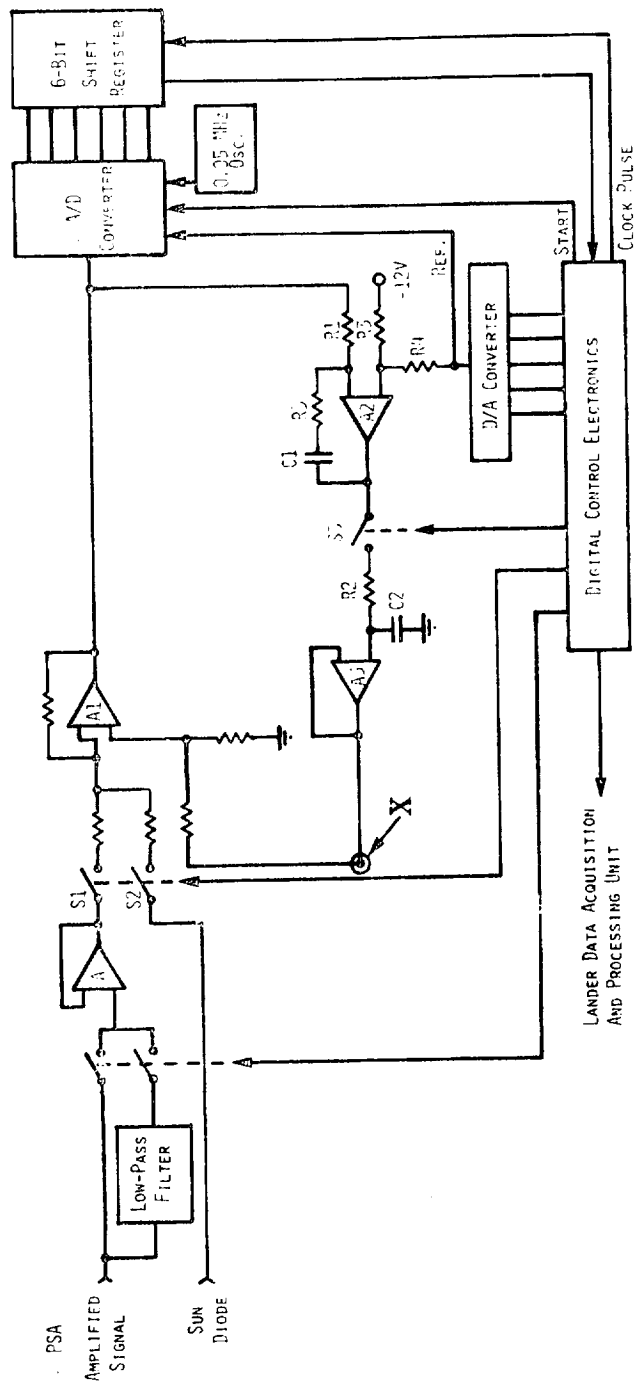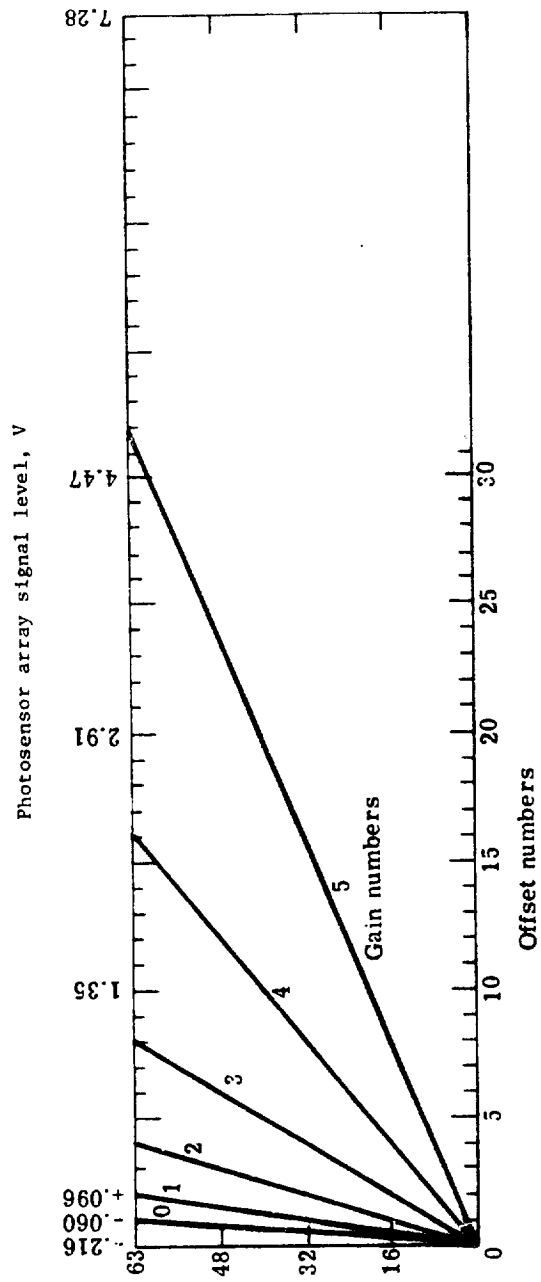
Figure 3.— Simplified circuit diagram of the video processing electronics.

Figure 4.- Nominal gains and offsets.
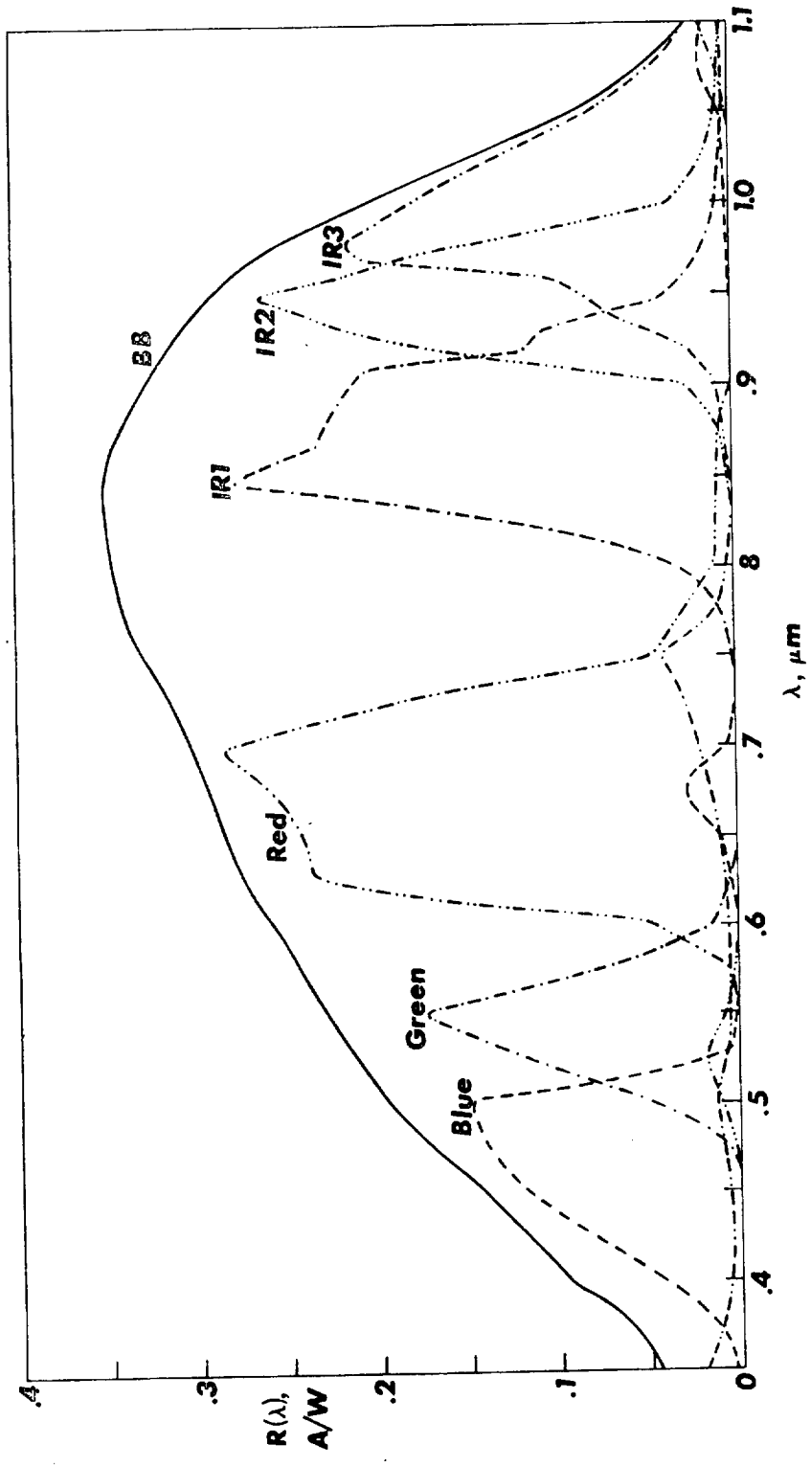
Figure 5.- Typical photosensor array responsivities.

Figure 6.- Reference test chart.